Hole Transport in Poly[2,7-(9,9-dihexylfluorene)-*alt*-bithiophene] and High-Efficiency Polymer Solar Cells from Its Blends with PCBM

Weihua Tang,*,†,‡ Vijila Chellappan,† Minghui Liu,§ Zhi-Kuan Chen,† and Lin Ke*,†

Institute of Materials Research and Engineering, 3 Research Link, Singapore 117602, Singapore, and Department of Chemistry, National University of Singapore, Singapore 117543, Singapore

ABSTRACT We report herein a detailed study of the thermal and hole-transport properties of poly[2,7-(9,9-dihexylfluorene)-*alt*-bithiophene] (F6T2) and its photovoltaic performance in a bulk-heterojunction (BHJ) solar cell. This crystalline polymer has a high weight-average molecular weight ($M_w = 52\ 400$) with a polydispersity index of 1.99. With a band gap of 2.36 eV, F6T2 exhibits strong absorption in the 300−500 nm region. BHJ solar cells blending F6T2 with [6,6]-phenyl-C_{61}-butyric acid methyl ester (PCBM) (1:3 weight ratio) as the active layer present a high open-circuit voltage ($V_{oc} \sim 0.9$ V) and a promising power conversion efficiency of 2.4% under simulated solar light AM1.5G (100 mW/cm^2). Furthermore, F6T2 shows sufficient hole mobility [ca. 8.4×10^{-5} cm^2/(V s) at 310 K and 2.5×10^5 V/cm applied electric field] by a time-of-flight transient photocurrent technique, allowing efficient charge extraction and a good fill factor for solar cell application. Nanoscale phase separation was observed in F6T2/PCBM films with a surface roughness lower than 60 nm.

KEYWORDS: solar cell • charge transport • poly[2,7-(9,9-dihexylfluorene)-*alt*-bithiophene] • time-of-flight technique • photo-CELIV technique

1. INTRODUCTION

The pursuit of inexpensive renewable energy sources has stimulated scientific research for efficient photovoltaic devices (1). Polymer solar cells have shown the potential to harness solar energy in a cost-effective way because of their low fabrication cost, ease of processing, mechanical flexibility (2−7), and versatility in manipulating chemical structures (8−10). Since the pioneering work from Heeger's group in 1995 (11), the power conversion efficiency (PCE) of polymer solar cells has impressively improved based on the so-called bulk-heterojunction (BHJ) concept structure, where a photoactive layer is formed by the interpenetrating network of π-conjugated polymer donors and soluble fullerenes (12) or nanocrystal acceptors (13). The most successful system reported to date is a blend of regioregular poly(3-hexylthiophene) (P3HT) and [6,6]-phenyl-C_{61}-butyric acid methyl ester (PCBM), the material combination that gives the highest reported PCE values (4−5%) (2, 14−16). Theoretically, the PCE of polymer solar cells can be further improved (ca. 10%) by implementing new materials and exploring new device architecture (15−18).

Some key issues of both materials and device development remain to be resolved, including how to improve the photon absorption and facilitate photoinduced charge separation and transport (19). One interesting approach is by narrowing the donor band gap to enhance light absorption. Recent developments on low-band-gap (<2.0 eV) polymers for photovoltaic applications are well reviewed (15, 16, 20−22). Such low-band-gap polymers as PCPDTBT (19), PTB1 (23), and PCDTBT (24) have demonstrated excellent photon harvesting and efficient photogeneration of charge-separated states when blending with PCBM. A further attractive approach to developing higher efficiency solar cells involves the stacking of multiple solar cells into a tandem structure, where each cell absorbs different parts of the sun spectrum (17, 25). In the fabrication of tandem cells, there is a great demand for wide-band-gap polymers like P3HT to effectively capture higher energy light with wavelengths below 600 nm. The most successful tandem cell reported so far achieved an efficiency of 6.5% with PCPDTBT stacked with P3HT (17). To date, only a few polymers have demonstrated high PCE in the 300−600 nm absorption region. Examples are a two-dimensional polythiophene with bis(thienylenevinylene) side chains (biTV-PT) reported by Hou et al. (26) and a polyfluorene copolymer with a thienylbenzothiadiazole moiety (PFDTBT) from Inganäs' group (27). The former polymer achieved a 1.71% PCE at its strongest absorption between 300 and 500 nm, with the latter one gaining 2.5% efficiency in the range from 400 to 600 nm.

In our recent pursuit of polymer light-emitting diodes (PLEDs), an alternating copolymer of fluorene and bithiophene, poly[2,7-(9,9-dihexylfluorene)-*alt*-bithiophene] (F6T2), was developed, and it exhibited good device stability and high charge-transport properties (28, 29). Our exploration of F6T2 potential in BHJ solar cells was inspired by its dioctyl analogue poly[2,7-(9,9-dioctylfluorene)-*alt*-bithiophene] (F8T2).

* E-mail: karen-kl@imre.a-star.edu.sg (L.K.), tang-wh@hotmail.com (W.T.).
Received for review March 11, 2009 and accepted May 18, 2009
† Institute of Materials Research and Engineering.
‡ Present address: College of Chemical Engineering, Nanjing University of Science and Technology, Nanjing 210094, People's Republic of China.
§ National University of Singapore.
DOI: 10.1021/am900144b

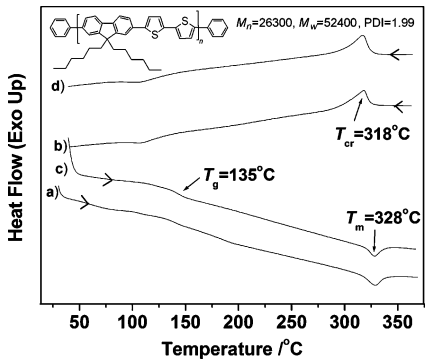

FIGURE 1. DSC thermograms of F6T2 in two continuous thermal cycles: (a) heating at 20 °C/min of the pristine sample; (b) slow cooling at 10 °C/min after equilibration at 370 °C; (c) heating at 20 °C/min after slow cooling from 370 °C; (d) slow cooling at 10 °C/min after equilibration at 370 °C. The inset shows the structure of F6T2 and its molecular weight.

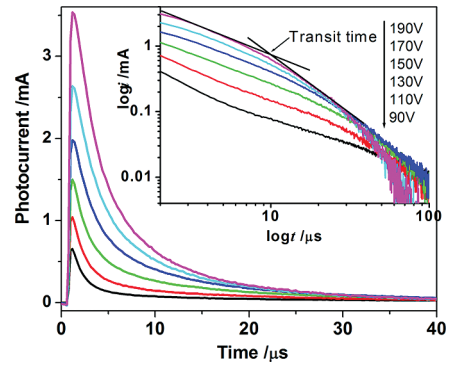

FIGURE 2. TOF photocurrent transient for hole transport in F6T2 films at different applied voltages in a linear plot recorded at 310 K. The inset shows the log i−log t plots of F6T2 films at different applied voltages.

This analogue has displayed relatively high charge mobility [2×10^{-3} cm^2/(V s)] in a thin-film transistor (30) and promising results in BHJ solar cells with nanoporous TiO_2 (31) or with PCBM (32). Herein, the combination of superior charge transport of polyfluorene-based materials (30, 33, 34) and the good match of spectral response to solar emission spectra, as exhibited by F6T2, is very intriguing to us and thus motivated this study on its potential application in BHJ solar cells.

In this paper, the thermal and charge-transport properties and photovoltaic performance of high-molecular-weight F6T2 are studied in detail. The hole transport in F6T2 films is investigated using a time-of-flight (TOF) technique (35). Weakly dispersive hole mobility is observed in a F6T2 film cast from chloroform at 310 K. The hole transport results are further analyzed using the Pool−Frenkel model (36, 37) and disorder formalism with Bässler's Gaussian disorder model (GDM) (38) and corrected disorder model (CDM) (39). The TOF study shows that F6T2 exhibits a hole mobility of 8.4×10^{-5} cm^2/(V s) at a 2.5×10^5 V/cm electric field, which is even higher than the value reported earlier for P3HT [5.1×10^{-5} cm^2/(V s)] (8, 9). The BHJ solar cells consisting of an active layer of F6T2/PCBM (1:3) sandwiched between metallic electrodes are fabricated and present promising PCE up to 2.4%.

2. RESULTS AND DISCUSSION

2.1. Thermal Properties of F6T2. The polymer F6T2 used in the current study was synthesized with a palladium-catalyzed Suzuki coupling reaction in our laboratory (28, 29). Possessed with a high-weight-average molecular weight (M_w = 52 400, PDI = 1.99, where PDI is polydispersity index) and a band gap of 2.36 eV, F6T2 exhibited strong absorption in the 300−500 nm region. The thermal-induced phase-transition behavior of this high-molecular-weight F6T2 was investigated by differential scanning calorimetry (DSC) with a two-cycle heating and cooling process (Figure 1). When heated, F6T2 presents a glass transition temperature (T_g) of around 135 °C and a melting temperature (T_m) at 328 °C (Figure 1a,c). Upon slow cooling from the melt state, clear recrystallization was observed to occur at around 318 °C (Figure 1b,d). In comparison with F8T2 (40), F6T2 possesses higher melting and recrystallization temperatures. A good thermal stability of F6T2 (a 5% weight loss occurred upon heating to 436 °C) was revealed by thermogravimetric analysis. The high decomposition and glass transition temperatures of F6T2 are adequate for its application in optoelectronic devices such as PLED and photovoltaic solar cells.

2.2. Hole Transport of F6T2. For solar cells, the charge transport in the polymer is crucial for efficient collection of photogenerated charges. Cyclic voltammetry studies indicate that F6T2 has an onset oxidation potential (φ_{ox}) of 0.73 V and a reduction potential (φ_{red}) of 1.76 V (28, 29). The highest occupied molecular orbital (HOMO) and lowest unoccupied molecular orbital (LUMO) energy levels were determined from φ_{ox} and φ_{red} to be −5.13 and −2.64 eV, respectively, when taking into account the self-consistent energy level at −4.4 eV (41), which are significantly higher than those of PCBM ($E_{HOMO} = -6.10$ eV; $E_{LUMO} = -3.70$ eV) (8, 9). The electron-transfer process from F6T2 to PCBM is thus expected to be favored. The hole-transport property of F6T2 was investigated by using a TOF photoconductivity technique, where F6T2 films were drop-casted from a chloroform solution onto an indium−tin oxide (ITO)-coated glass substrate. Using the same experimental setup and measurement method as those reported before (42), the temperature- and electric-field-dependent charge mobility of F6T2 was investigated. The TOF photocurrent transients for the holes (Figure 2) were recorded using F6T2/ITO as the charge carrier generation layer. When calculated, the charge mobility using the relation $\mu = L^2/Et_\tau$ (where L is the polymer film thickness, E the applied voltage, and t_τ the transient time), the hole mobility of F6T2 at 310 K was found to be 8.4×10^{-5} cm^2/(V s) at an applied electric field of 2.5×10^5 V/cm. Compared with other widely used hole-transport materials, this hole mobility is relatively higher than that of fast-grown P3HT films [5.1×10^{-5} cm^2/(V s)] (8, 9) and even 1 order of magnitude higher than the reported value for MEH-PPV [1.7×10^{-6} cm^2/(V s)] (39), while 1 order of magnitude lower than that of poly(9,9-dioctylfluorene) (PFO) [$\sim 3 \times 10^{-4}$ cm^2/(V s)] at 2.5×10^5 V/cm (44). In comparison with the thin-film mobility [2×10^{-3} cm^2/(V s)] of a F8T2

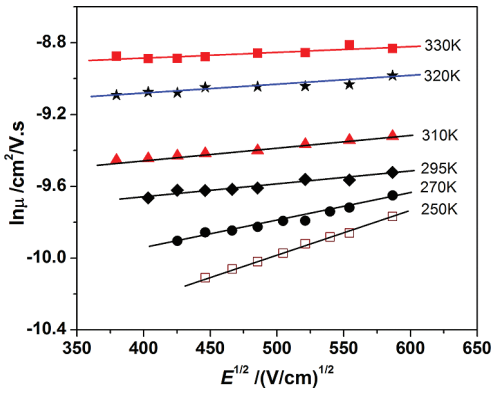

FIGURE 3. Electric-field-dependent TOF hole mobility of F6T2 at temperatures from 250 to 330 K. The solid lines are the fit according to the Poole−Frenkel relation.

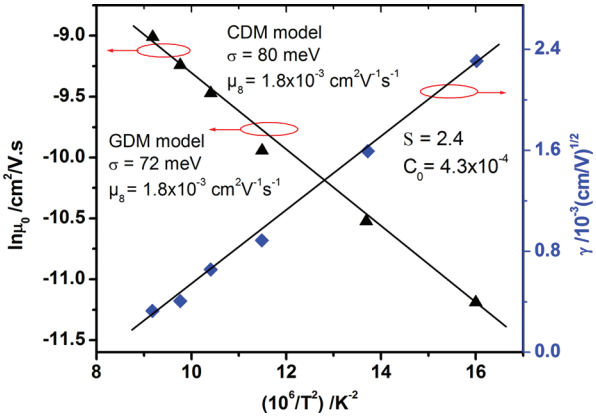

FIGURE 4. Temperature dependence of the logarithmic zero-field mobility (μ_0) (solid triangles) in F6T2 and the slope of the field dependence of mobility (γ) (solid squares). The lines are linear fits to the data.

field-effect transistor (30), the thick-film mobility of F6T2 measured from a TOF technique was 2 orders of magnitude lower. This may be due to unaligned F6T2 polymer chains in thick films and higher resistance for holes in traveling cross the thick films, while a F8T2 thin-film mobility was achieved with aligned polymer chains.

An insight into the hole-transport properties of F6T2 was achieved by investigating its electric-field-dependent hole mobility with a gradual increase in the temperature from 250 to 330 K at intervals of 10−25 K. A plot of ln μ against $E^{1/2}$ at different temperatures is shown in Figure 3. A linear relationship is observed and agrees well with the Poole−Frenkel equation (37)

$$\ln\left(\frac{\mu_E}{\mu_{E=0}}\right) = \gamma E^{1/2} \qquad (1)$$

where γ is the slope of the field dependence of the charge mobility and μ_0 ($\mu_{E=0}$) is the zero-field mobility.

As shown in Figure 4, the zero-field mobility (μ_0) increases with temperature while the slope γ decreases with increasing temperature, which is characteristic for hopping transport in disordered organic solids. When charges transport in disordered organic materials by hopping, we can describe

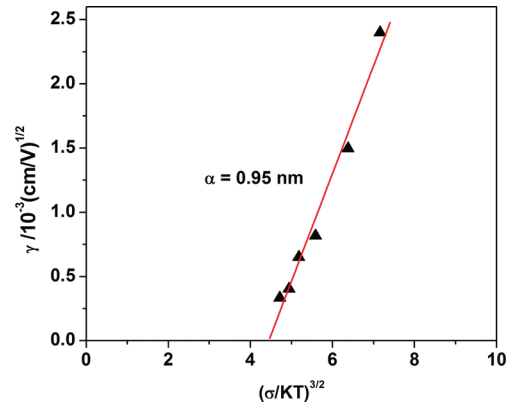

FIGURE 5. Slope of the field dependence of mobility (γ) versus (σ/kT)$^{3/2}$. The solid line is a linear fit to the data.

it with a disorder formalism, assuming that charge transport takes place by hopping through a manifold of localized states subject to fluctuation of both the hopping site energy and intermolecular distance following the Gaussian distributions. In the GDM (38), the mobility can be expressed as

$$\mu_{GDM} = \mu_\infty \exp\left[-\left(\frac{2\sigma}{3kT}\right)^2\right] \exp\left\{C\left[\left(\frac{\sigma}{kT}\right)^2 - \Sigma^2\right]E^{1/2}\right\} \qquad (2)$$

where μ_∞ is the high-temperature limit of the charge mobility and C is an empirical constant. The energetic disorder parameter σ arises from distribution of the conjugation length, while the positional disorder parameter Σ arises from fluctuation of the intermolecular distances or morphological variations. By plotting ln μ_0 against $10^6/T^2$ (Figure 4) and conducting a linear fit according to eq 2, we can obtain the GDM parameters as $\mu_\infty = 1.8 \times 10^{-3}$ cm^2/(V s) and $\sigma_{GDM} =$ 72 meV. The positional disorder parameter Σ and the empirical constant C are obtained from the linear fit of the curves by plotting γ against $10^6/T^2$ (Figure 4). The parameters Σ and C are found to be $\Sigma = 2.4$ and $C = 4.3 \times 10^{-4}$ (cm/V)$^{1/2}$. The intersite hopping constant C is approximately 3 times smaller than the value reported for MEH-PPV [1.7×10^{-3} (cm/V)$^{1/2}$] (39) but slightly larger than the value reported for PFO [2.5×10^{-4} (cm/V)$^{1/2}$] (44). This indicates that hole transport by hopping in F6T2 and PFO is much easier than that in MEH-PPV and comparable to that in PFO.

Considering long-range correlations between hopping sites due to charge−dipole interaction, the temperature- and field-dependent charge mobility can also be described with the CDM (39),

$$\mu_{CDM} = \mu_\infty \exp\left[-\left(\frac{3\sigma}{5kT}\right)^2\right] \exp\left[0.78\left\{\left(\frac{\sigma}{kT}\right)^{3/2} - 2\right\}\sqrt{\frac{eaE}{\sigma}}\right] \qquad (3)$$

where a is the intersite spacing. The average hopping distance a is obtained from the linear fit of the plot of γ against $(\sigma/kT)^{3/2}$ (Figure 5) and is estimated to be 0.95 nm. The energetic disorder parameter σ_{CDM} was calculated from

Table 1. Photovoltaic Performance of F6T2:PCBM (1:3) BHJ Solar Cells on a ITO-Coated Glass Substrate and 40 nm PEDOT:PSS as the Hole-Injection Layer with Different Metal Cathodes and Thicknesses of Active Layers without Annealing

photovoltaic device configuration	EQE (%)	J_{sc} (mA/cm^2)	V_{oc} (V)	FF (%)	PCE (%)
ITO/PEDOT:PSS/F6T2:PCBM (70 nm)/LiF (0.7 nm)/Al (100 nm)	63	5.12	0.96	0.49	2.4
ITO/PEDOT:PSS/F6T2:PCBM (70 nm)/Ca (20 nm)/Ag (80 nm)	63	4.38	0.87	0.52	2.0
ITO/PEDOT:PSS/F6T2:PCBM (50 nm)/Ca (20 nm)/Ag (80 nm)	63	4.92	0.86	0.54	2.3

the linear plot of ln μ_0 against $10^6/T^2$ (Figure 4) and found to be 80 meV and μ_∞ to be 1.8×10^{-3} cm^2/(V s). With the derived values of σ_{CDM}, μ_∞, and a in hand, the localization length for charges L can be estimated using the relation

$$\mu_\infty = \frac{ea^2\upsilon_{ph}}{\sigma}\exp(-2a/L) \qquad (4)$$

where υ_{ph} is the phonon frequency for hopping ($\sim 10^{12}$ s^{-1}). L is found to be 4.6 Å, which is similar to that of BPPPV-PF (3.6 Å) (42). This localization length is comparable with those obtained from structurally regular, chemically pure conjugated polymers (43).

By the above-discussed TOF mobility measurement, F6T2 showed relatively high hole-charge-transport mobility [8.4×10^{-5} cm^2/(V s) at 310 K and 2.5×10^5 V/cm applied electric field] at unaligned polymer chain conditions. The hopping process in hole transport is easier than that for MEH-PPV and occurs with a reasonable localization length like chemically pure and structurally regular polymers.

2.3. Photovoltaic Performance of F6T2. The BHJ solar cells were fabricated with a configuration of either ITO/PEDOT:PSS/F6T2:PCBM/LiF/Al or ITO/PEDOT:PSS/F6T2:PCBM/Ca/Ag (refer to the Experimental Section). The active layers of all devices were spin-coated from a mixture solution of F6T2/PCBM (1:3, w/w) in 1,2-dichlorobenzene without thermal annealing. The $J-V$ characteristic of devices was measured under a N_2 atmosphere. The thickness of the active layer was controlled by the spin-coating rate and the concentration of the F6T2/PCBM solution. Table 1 summarizes the photovoltaic performance of F6T2/PCBM devices. The $J-V$ curve of a typical device is plotted in Figure 6, with an inset showing the external quantum efficiency

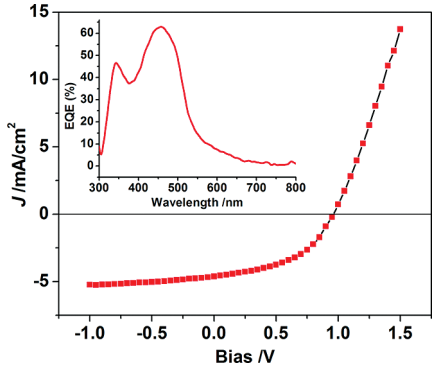

FIGURE 6. $J-V$ curve of solar cells from ITO/PEDOT:PSS/F6T2:PCBM (1:3) (70 nm)/LiF (0.7 nm)/Al (100 nm) under AM1.5G illumination at an irradiation intensity of 100 mW/cm^2. The inset shows the EQE of the device, with a maximum EQE reaching as high as 63%.

(EQE) variation with the wavelength. The F6T2/PCBM solar cell shows high EQE values in all devices, with a maximum EQE reaching 63% at 457 nm and a EQE of over 40% in the range from 330 to 500 nm. The F6T2 cells achieve the highest AM1.5G PCE of 2.4%, with an open-circuit voltage (V_{oc}) of 0.96 V, a short-circuit current density (J_{sc}) of 5.12 mA/cm^2, and a fill factor (FF) of 0.49. These data are very close to the best values, $J_{sc} = 4.24$ mA/cm^2, $V_{oc} = 0.99$, FF = 0.51, and PCE = 2.14%, achieved from a solar cell with a F8T2 and PCBM (1:1) blend after annealing at 70 °C from a 1,2,4-trichlorobenzene spin-coated film (32). The PCE of the F6T2 cell is reproducible, and the values are from 2.0 to 2.4% from 12 individual solar cells with those three table-listed different configurations.

Solar cells present particularly high open-circuit voltages ($V_{oc} \sim 0.90$ V) and relatively high fill factors (FF ~ 0.50) and thus display very promising PCE ($\eta \sim 2.4\%$). V_{oc} of the F6T2/PCBM solar cells ranges from 0.86 to 0.96 V, ca. 0.3−0.4 V higher than that of P3HT, which benefited from the high oxidation potential of F6T2. According to the design rule for the donor polymer in the BHJ solar cell, V_{oc} of the cell can be estimated by the HOMO energy level of the conjugated polymer and the LUMO energy level of PCBM (18). By taking into account a LUMO level for PCBM at −3.7 eV for the semiempirical estimation equation (8, 9, 18), V_{oc} of our F6T2/PCBM solar cell was estimated to be 1.13 V, which is slightly higher than our experimental values, indicating that the performance of our cells can be pushed further with higher V_{oc}.

Interestingly, the insertion of a thin interlayer of LiF (0.7 nm) under an Al cathode significantly enhances the short-circuit current density, stabilizes high open-circuit voltages of our F6T2 cells, and thus gives a better photovoltaic performance. This positive influence of a thin layer of LiF was also observed in other polythiophene (45) and poly[2-methoxy-5-(3′,7′-dimethyloctyloxy)-1,4-phenylenevinylene] solar cells (46, 47).

In comparison with the well-established P3HT/PCBM cells (8, 9, 14−16), our F6T2 cells are relatively lower in J_{sc}, which we believe to be attributed to its lower hole mobility. It is widely believed that the fundamental limitation of the photocurrent of PCBM-based BHJ solar cells lies in the low mobility of the holes in the donor polymer (48). An understanding of the hole mobility of F6T2/PCBM (1:3) blends in BHJ solar cells is achieved by using photoinduced charge carrier extraction by a linearly increasing voltage (photo-CELIV) technique (49). The sample consists of a thin layer (70 nm) of F6T2:PCBM sandwiched between a transparent ITO-coated glass and evaporated Al electrodes, which is the

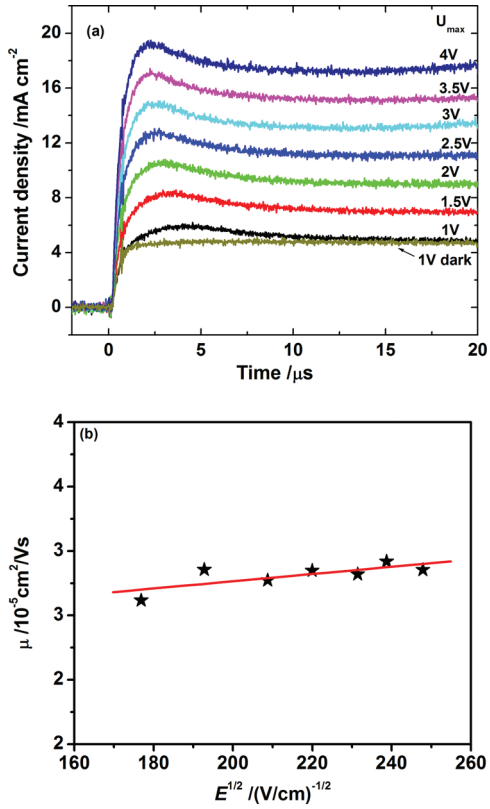

FIGURE 7. (a) Photo-CELIV transients in a F6T2/PCBM blend (1:3, w/w) film recorded at 298 K by changes in the maximum of the applied voltage pulse. (b) Variation of the charge mobility with the applied electric field.

typical structure of the BHJ solar cell. The hole mobility can be estimated as $\mu = 2d^2/3At_{max}^2[1 + 0.36\Delta j/j(0)]$, where d is the thickness of the film, A is the voltage rise speed (A = voltage applied/t_{pulse}), $j(0)$ is the capacitive displacement current, Δj is the current due to the photogenerated carriers, and t_{max} is the characteristic extraction time (50). Figure 7 presents the variation of photo-CELIV transients with applied voltages (U_{max}) at fixed light intensity and delay time (20 μs). As shown, t_{max} elongates as the maximum of the voltage pulse is decreased, which is related to the field dependence of the mean velocity of the charge carriers (49). The electric-field-dependet mobility (μ) with varied E is presented by plotting μ against the square root of the electric field ($E^{1/2}$) (Figure 7b). The hole mobility in the F6T2/PCBM (1:3) film is observed to increase linearly with an increase in the applied electric field, following the Poole−Frenkel equation. The hole mobility through the F6T2/PCBM blend is found to be 3.4×10^{-5} cm^2/(V s) at 298 K and an electric field of 4.84×10^4 V/cm (Figure 7b). This hole mobility is on the same order of magnitude as the one measured by the TOF technique.

From the study of F8T2, the hole mobility of the donor polymers can be enhanced by aligning the polymer chains in the liquid-crystalline phase (51). Our polymer F6T2 shows crystallinity from DSC analysis. The existence of this crystallinity in the F6T2/PCBM blend is a key issue to understanding the moderate J_{sc} in a solar cell. From the preliminary X-ray diffraction (XRD) measurements on the F6T2/PCBM blend film spin-coated on an ITO-coated glass substrate, we could

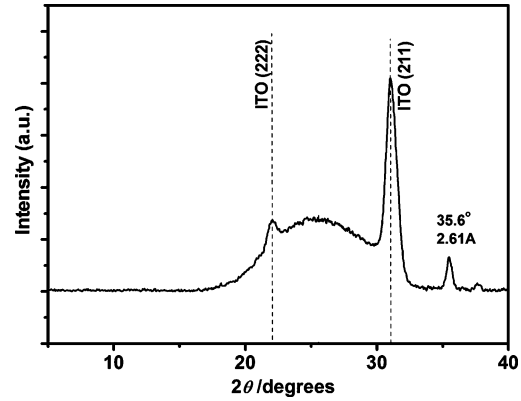

FIGURE 8. XRD of the F6T2/PCBM blend film on an ITO-coated glass substrate such as for the solar cell device.

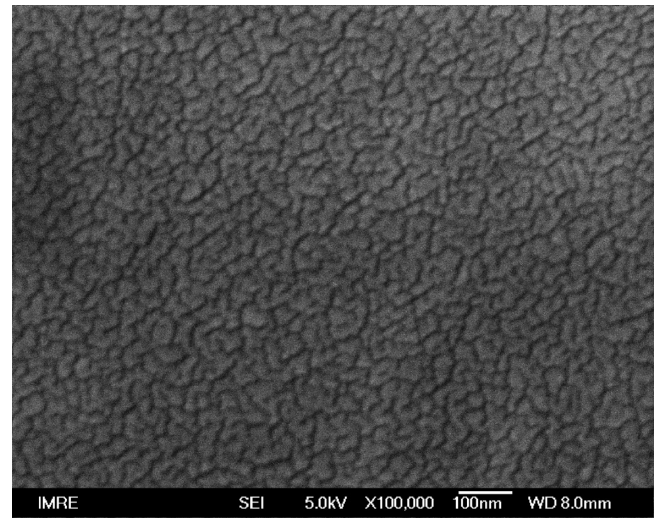

FIGURE 9. SEM image (top view) of a F6T2/PCBM (1:3) thin film on an ITO substrate.

not clearly indentify the crystalline peaks from F6T2 (Figure 8). The only small peak observed at $2\theta = 35.6°$, corresponding to a distance $d = 2.61$ Å, can possibly be assigned for F6T2. This indicates that F6T2 polymer chains can only achieve short-distance ordered alignment within the repetition units along single polymer chains, while the bulk polymer films are mostly amorphous. A high-degree ordered structure for the F6T2/PCBM blend film may be further achieved by thermal annealing or solvent evaporation (8, 9).

Achieving nanoscale phase separation within the donor polymer and PCBM blend is beneficial for high-performance BHJ solar cells because this morphology enables a large interface area for exciton dissociation and a continuous percolation path for hole and electron transport to the corresponding electrodes (52). Figure 9 shows a scanning electron microscopy (SEM) image of a F6T2/PCBM blend film, which does show distinct phase separation and represents traditional bulk heterojunctions of PT and the fullerene. The main morphological feature of the blend film shows a homogeneous nanoscale distribution of two components. The dark areas are attributed to PCBM-rich domains (52) with average size lower than 50 nm. The bright F6T2 domains show interpenetrating networks with PCBM domains, allowing better percolation of hole carriers. The

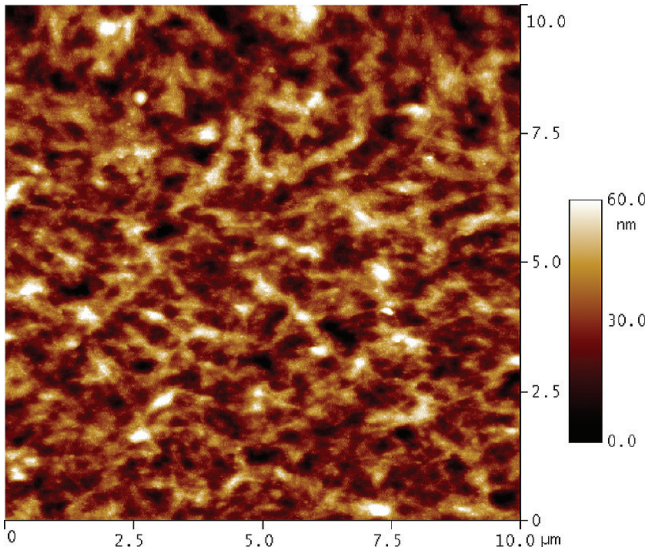

FIGURE 10. AFM image of the surface morphology of a F6T2/PCBM (1:3) thin film.

atomic force microscopy (AFM) image (Figure 10) also exhibits very fine domains, and no large phases can be found. The film presented the largest peak-to-valley height of around 30 nm, corresponding to ~50% of the mean thickness, and a root-mean-square (rms) roughness (24) of around 1 nm. This nanoscale phase separation and interpenetrating network morphology between the electron donor polymer (F6T2) and acceptor material (PCBM) allow a large area of the interface for better photogenerated charges and desirable J_{sc}. However, the possibility of a recombination of hole and electron carriers at these high interfacial areas could also be enhanced. This might be the reason why the J_{sc} values of F6T2 devices have not reached their utmost values. Indeed, it is a challenge to achieve the properly organized morphology of a polymer/fullerene blend in the active layers of BHJ solar cells in order to push further the optimum performance. Further exploration of morphology control and tandem cells is ongoing and will be reported in due time.

3. CONCLUSIONS

In this paper, the crystalline polymer F6T2 shows high hole mobility, in the range of 8.4×10^{-5} cm^2/(V s) at 2.5×10^5 V/cm applied electric field. The simple solar cells prepared by blending of this polymer and fullerene exhibit a high PCE of 2.4%, a high open-circuit voltage (~0.9 V), and a relatively high FF of around 50%. XRD analysis found that the crystallinity of F6T2 was suppressed in the F6T2/PCBM blends without special treatments. The crystallinity of F6T2, morphology of F6T2/PCBM, and therefore FF of the BHJ solar cells can be further improved by exploring suitable post-treatment in device fabrication such as solvent annealing and solvent evaporation. Considering the significant improvement in BHJ solar cells like the P3HT/PCBM blend through device engineering, F6T2 stands out as a promising candidate in harvesting solar energy in the 300−500 nm region for further exploration in tandem cells.

4. EXPERIMENTAL SECTION

The hole mobility of F6T2 films was characterized using TOF photoconductivity measurement with a device architecture of ITO/F6T2/Al. A thick F6T2 film was prepared by drop-casting its solution in chloroform (10 mg/mL) onto the patterned ITO glass substrate in a saturated solvent environment and further annealing at 60 °C for 3 h in a N_2 environment to remove any residual solvent. Afterward, the Al electrode (100 nm) was evaporated onto the polymer film by an ULVAC evaporation system. The device active area was 4 mm^2. The film thickness was determined after the TOF photoconductivity measurement using a surface profiler (KLA-Tencor P10 surface profiler) and found to be 5.5 μm. The TOF measurement system consists of a pulsed N_2 laser (Oriel 79074), a pulse generator (SRS-DG535), a direct-current voltage source, and a digital oscilloscope (Agilent-Infiniium, 1 GHz, 4 GSa/s). The sample was housed in a temperature-controlled continuous-flow cryostat under a vacuum pressure of $\sim 1 \times 10^{-3}$ Pa. The laser (pulse width < 4 ns; pulse repetition rate = 1 Hz) was shot on the ITO side of the device. Variation of the photocurrent with the applied electric field was monitored through a variable resistor using an oscilloscope, and care was taken to ensure that the time constant of the setup was less than the transit time ($RC < t_t$). The transit times were obtained from the intersection of the asymptotes to the plateau and the declining slope of the logarithmic plot of the transient signal.

The photo-CELIV measurement was carried out by generating the charge carriers using a pulsed N_2 laser (337.1 nm) and extracting the charges using a linearly increasing voltage ramp at a fixed delay between the laser pulse and the voltage ramp. The ramp voltages of different amplitudes and pulse widths were applied to the test devices in order to study the field dependence of charge mobility in the electron donor−acceptor composition.

BHJ polymer solar cells were prepared with a configuration of either ITO/PEDOT:PSS/F6T2:PCBM/LiF/Al or ITO/PEDOT:PSS/F6T2:PCBM/Ca/Ag. Hole-injection layer PEDOT:PSS with 40 nm thickness was spin-coated onto a UV-ozone-treated ITO-coated glass substrate. A single photoactive layer was built by spin-coating mixture solutions of F6T2 and PCBM (weight ratio 1:3) in 1,2-dichlorobenzene. A LiF or Ca layer was further deposited on the top of the blend film, followed by deposition of an Al or Ag layer as the cathode. The solar cells were sealed inside a glovebox to give an effective area of 9 mm^2. All device preparation and characterization were performed under a N_2 atmosphere without annealing. The current density−voltage ($J-V$) characteristics of the polymer solar cells were measured using a simulated AM1.5G illumination of 100 mW/cm^2 (Steuernagel 535) and a Keithley 2400 Source/Measure unit. DSC was performed on a TA 2920 modulated DSC instrument with a heating rate of 20 °C/min and a cooling rate of 10 °C/min. The crystallinity of the F6T2/PCBM blend was studied with a high-resolution X-ray diffractometer (Panalytical). The phase separation morphology of rgw F6T2/PCBM film was characterized by using a scanning electron microscope (JSM-5600) and a tapping-mode atomic force microscope (Veeco Instruments Inc.).

REFERENCES AND NOTES

(1) Günes, S.; Neugebauer, H.; Sariciftci, N. S. *Chem. Rev.* **2007**, *107*, 1324.
(2) Lungenschmied, C.; Dennler, G.; Neugebauer, H.; Sariciftci, S. N.; Glatthaar, M.; Meyer, T.; Meyer, A. *Sol. Energy Mater. Sol. Cells* **2007**, *91*, 379.
(3) Krebs, F. C.; Spanggard, H.; Kjær, T.; Biancardo, M.; Alstrup, J. *Mater. Sci. Eng., B* **2007**, *138*, 106.
(4) Niggemann, M.; Zimmermann, B.; Haschke, J.; Glatthaar, M.; Gombert, A. *Thin Solid Films* **2008**, *516*, 7181.
(5) Krebs, F. C.; Jørgensen, M.; Norrman, K.; Hagemann, O.; Alstrup, J.; Nielsen, T. D.; Fyenbo, J.; Larsen, K.; Kristensen, J. *Sol. Energy Mater. Sol. Cells* **2009**, *93*, 422.

(6) Krebs, F. C. *Sol. Energy Mater. Sol. Cells* **2009**, *93*, 465–475.
(7) Blankenburg, L.; Schultheis, K.; Schache, H.; Sensfuss, S.; Schrödner, M. *Sol. Energy Mater. Sol. Cells* **2009**, *93*, 476.
(8) Li, G.; Shrotriya, V.; Huang, J.; Yao, Y.; Moriarty, T.; Emery, K.; Yang, Y. *Nat. Mater.* **2005**, *4*, 864.
(9) Shrotriya, V.; Li, G.; Yao, Y.; Chu, C.-W.; Yang, Y. *Appl. Phys. Lett.* **2006**, *88*, 073508.
(10) Brabec, C. J. *Sol. Energy Mater. Sol. Cells* **2004**, *83*, 273.
(11) Yu, G.; Gao, J.; Hemmelen, J. C.; Wudl, F.; Heeger, A. J. *Science* **1995**, *270*, 1789.
(12) Thompson, B. C.; Fréchet, J. M. J. *Angew. Chem., Int. Ed.* **2008**, *47*, 58.
(13) Bouclé, J.; Ravirajan, P.; Nelson, J. *J. Mater. Chem.* **2007**, *17*, 3141.
(14) Ma, W.; Yang, C.; Gong, X.; Lee, K.; Heeger, A. J. *Adv. Funct. Mater.* **2005**, *15*, 1617.
(15) Lee, J. Y.; Kim, S. H.; Lee, H.-H.; Lee, K.; Ma, W.; Gong, X.; Heeger, A. J. *Adv. Mater.* **2006**, *18*, 572.
(16) Chen, C.-P.; Chan, S.-H.; Chao, T.-C.; Ting, C.; Ko, B.-T. *J. Am. Chem. Soc.* **2008**, *130*, 12828.
(17) Kim, J. Y.; Lee, K.; Coates, N. E.; Moses, D.; Nguyen, T.-Q.; Dante, M.; Heeger, A. J. *Science* **2007**, *317*, 222.
(18) Scharber, M. C.; Mühlbacher, D.; Koppe, M.; Denk, P.; Waldauf, C.; Heeger, A. J.; Brabec, C. J. *Adv. Mater.* **2006**, *18*, 789.
(19) Soci, C.; Hwang, I.-W.; Moses, D.; Zhu, Z.; Waller, D.; Gaudiana, R.; Brabec, C. J.; Heeger, A. J. *Adv. Mater.* **2007**, *17*, 632.
(20) Bundgaard, E.; Krebs, F. C. *Sol. Energy Mater. Sol. Cells* **2007**, *91*, 954.
(21) Kroon, R.; Lenes, M.; Hummelen, J. C.; Blom, P. W. M.; de Boer, B. *Polym. Rev.* **2008**, *48*, 531.
(22) Krebs, F. C. *Sol. Energy Mater. Sol. Cells* **2009**, *93*, 394.
(23) Liang, Y.; Wu, Y.; Feng, D.; Tsai, S.-T.; Son, H.-J.; Li, G.; Yu, L. *J. Am. Chem. Soc.* **2009**, *131*, 56.
(24) Blouin, N.; Michaud, A.; Leclerc, M. *Adv. Mater.* **2007**, *19*, 2295.
(25) Gilot, J.; Wienk, M. M.; Janssen, R. A. J. *Appl. Phys. Lett.* **2007**, *90*, 143512.
(26) Hou, J. H.; Tan, Z. A.; Yan, Y.; He, Y. J.; Yang, C. H.; Li, Y. F. *J. Am. Chem. Soc.* **2006**, *128*, 4911.
(27) Svensson, M.; Zhang, F.; Veenstra, S. C.; Verhees, W. J. H.; Hummelen, J. C.; Kroon, J. M.; Inganäs, O.; Andersson, M. R. *Adv. Mater.* **2003**, *15*, 988.
(28) Tang, W.; Ke, L.; Tan, L.; Kietzke, T.; Chen, Z.-K. *Macromolecules* **2007**, *40*, 6164.
(29) Ke, L.; Tang, W.; Song, Y.; Chen, Z.-K.; Chua, S. J. *J. Appl. Phys.* **2007**, *102*, 063103.
(30) Sirringhaus, H.; Kawase, T.; Friend, R. H.; Shimoda, T.; Inbasekaran, M.; Wu, W.; Woo, E. P. *Science* **2000**, *290*, 2123.
(31) Ravirajan, P.; Haque, S. A.; Durrant, J. R.; Poplavskyy, D.; Bradley, D. D. C.; Nelson, J. *J. Appl. Phys.* **2004**, *95*, 1473.
(32) In the preparation of our manuscript, the BHJ solar cells through blending of F8T2 and PCBM were reported to achieve 2.14% efficiency after annealing of the device at 70 °C for 20 min: Huang, J.-H.; Yang, C.-Y.; Ho, Z.-Y.; Kekuda, D.; Wu, M.-C.; Chien, F.-C.; Chen, P.; Chu, C.-W.; Ho, K.-C. *Org. Electron.* **2009**, *10*, 27.
(33) Sherf, U.; List, E. J. W. *Adv. Mater.* **2002**, *14*, 477.
(34) Schulz, L. G.; Chen, X.; Holdcroft, S. *Appl. Phys. Lett.* **2009**, *94*, 023302.
(35) Campbell, I. H.; Smith, D. L.; Neef, C. J.; Ferraris, J. P. *Appl. Phys. Lett.* **1999**, *74*, 2809.
(36) Gill, W. D. *J. Appl. Phys.* **1972**, *43*, 5033.
(37) Frenkel, J. *Phys. Rev.* **1938**, *54*, 647.
(38) Bässler, H. *Phys. Status Solidi B* **1993**, *175*, 15.
(39) Inigo, A. R.; Tan, C. H.; Fann, W.; Huang, Y.-S.; Perng, G.-Y.; Chen, S. A. *Adv. Mater.* **2001**, *13*, 504.
(40) Lim, E.; Jung, B.-J.; Lee, J.; Shim, H.-K.; Lee, J.-I.; Yang, Y. S.; Do, L.-M. *Macromolecules* **2005**, *38*, 4531.
(41) de Leeuw, D. M.; Simenon, M. M. J.; Brown, A. R.; Einerhand, R. E. F. *Synth. Met.* **1997**, *87*, 53.
(42) (a) Chellappan, V.; Almantas, P.; Huang, C.; Chen, Z.-K.; Ronald, O.; Chua, S. J. *Org. Electron.* **2007**, *8*, 8. (b) Chellappan, V.; Bavani, B.; Huang, C.; Chen, Z.-K.; Zhen, C.; Auch, M. D. J.; Chua, S. J. *Chem. Phys. Lett.* **2005**, *414*, 393.
(43) Martens, H. C. F.; Blom, P. W. M.; Schoo, H. F. M. *Phys. Rev. B* **2000**, *61*, 7489.
(44) Redecker, M.; Bradley, D. D. C.; Inbasekaran, M.; Woo, E. P. *Appl. Phys. Lett.* **1998**, *73*, 1565.
(45) Gadisa, A.; Svensson, M.; Andersson, M. R.; Inganäs, O. *Appl. Phys. Lett.* **2004**, *84*, 1609.
(46) Brabec, C. J.; Shaheen, S. E.; Winder, C.; Sariciftc, N. S.; Denk, P. *Appl. Phys. Lett.* **2002**, *80*, 1288.
(47) Brabec, C. J.; Cravino, A.; Meissner, D.; Sariciftci, N. S.; Fromherz, T.; Rispens, M. T.; Sanchez, L.; Hummelen, J. C. *Adv. Funct. Mater.* **2001**, *11*, 374.
(48) Brabec, C. J. *Sol. Energy Mater. Sol. Cells* **2004**, *83*, 273.
(49) Mozer, A. J.; Dennler, G.; Sariciftci, N. S.; Westerling, M.; Pivrikas, A.; Österbacka, R.; Juška, G. *Phys. Rev. B* **2005**, *72*, 035217.
(50) Juška, G.; Arlauskas, K.; Vilinas, M.; Kočka, J. *Phys. Rev. Lett.* **2000**, *84*, 4946.
(51) Sirringhaus, H.; Wilson, R. J.; Friend, R. H.; Inbasekaran, M.; Wu, W.; Woo, E. P.; Grell, M.; Bradley, D. D. C. *Appl. Phys. Lett.* **2000**, *77*, 406.
(52) Yang, X.; Loos, J. *Macromolecules* **2007**, *40*, 1353.

AM900144B